# Subthalamic Nucleus Deep Brain Stimulation Modulates 2 Distinct Neurocircuits

**Lunhao Shen, MS**[#1,2,3], **Changqing Jiang, PhD**[#1], **Catherine S. Hubbard, PhD**[3], **Jianxun Ren, MS**[1,2], **Changgeng He, MS**[1,2], **Danhong Wang, MD, PhD**[2], **Louisa Dahmani, PhD**[2], **Yi Guo, MD**[4], **Yiming Liu, MD**[5], **Shujun Xu, MD**[5], **Fangang Meng, MD**[6], **Jianguo Zhang, MD**[6], **Hesheng Liu, PhD**[2,3], **Luming Li, PhD**[1,7,8,9]

[1]National Engineering Laboratory for Neuromodulation, School of Aerospace Engineering, Tsinghua University, Beijing, China

[2]Athinoula A. Martinos Center for Biomedical Imaging, Department of Radiology, Massachusetts General Hospital, Harvard Medical School, Charlestown, MA, USA

[3]Department of Neuroscience, Medical University of South Carolina, Charleston, SC, USA

[4]Peking Union Medical College Hospital, Beijing, China

[5]Qilu Hospital of Shandong University, Jinan, China

[6]Beijing Tiantan Hospital, Capital Medical University, Beijing, China

[7]Precision Medicine & Healthcare Research Center, Tsinghua–Berkeley Shenzhen Institute, Shenzhen, China

[8]IDG(International Data Group)/McGovern Institute for Brain Research at Tsinghua University, Beijing, China

[9]Institute of Epilepsy, Beijing Institute for Brain Disorders, Beijing, China

[#] These authors contributed equally to this work.

## Abstract

**Objective:** Current understanding of the neuromodulatory effects of deep brain stimulation (DBS) on large-scale brain networks remains elusive, largely due to the lack of techniques that can reveal DBS-induced activity at the whole-brain level. Using a novel 3T magnetic resonance

imaging (MRI)-compatible stimulator, we investigated whole-brain effects of subthalamic nucleus (STN) stimulation in patients with Parkinson disease.

**Methods:** Fourteen patients received STN-DBS treatment and participated in a block-design functional MRI (fMRI) experiment, wherein stimulations were delivered during "ON" blocks interleaved with "OFF" blocks. fMRI responses to low-frequency (60Hz) and high-frequency(130Hz) STN-DBS were measured 1, 3, 6, and 12 months postsurgery. To ensure reliability, multiple runs (48 minutes) of fMRI data were acquired at each postsurgical visit. Presurgical resting-state fMRI (30 minutes) data were also acquired.

**Results:** Two neurocircuits showed highly replicable, but distinct responses to STN-DBS. A circuit involving the globus pallidus internus (GPi), thalamus, and deep cerebellar nuclei was significantly activated, whereas another circuit involving the primary motor cortex (M1), putamen, and cerebellum showed DBS-induced deactivation. These 2 circuits were dissociable in terms of their DBS-induced responses and resting-state functional connectivity. The GPi circuit was frequency-dependent, selectively responding to high-frequency stimulation, whereas the M1 circuit was responsive in a time-dependent manner, showing enhanced deactivation over time. Finally, activation of the GPi circuit was associated with overall motor improvement, whereas M1 circuit deactivation was related to reduced bradykinesia.

**Interpretation:** Concurrent DBS-fMRI using 3T revealed 2 distinct circuits that responded differentially to STN-DBS and were related to divergent symptoms, a finding that may provide novel insights into the neural mechanisms underlying DBS.

## Introduction

Subthalamic nucleus deep brain stimulation (STN-DBS) has become a well-established therapeutic intervention for Parkinson disease (PD),[1,2] which can result in significant motor improvement[3,4] that remains effective many years after implantation.[5] However, the exact neural mechanisms of how DBS impacts large-scale brain networks, and how the brain responds to varying stimulation frequencies over time, are still unclear.[6] A lack of understanding of the neural mechanisms underlying DBS treatment effects has hampered the development of efficient strategies for patient management, which requires careful programming of DBS parameters, a procedure that is largely based on subjective experience. More broadly speaking, a sophisticated understanding of how the brain responds to DBS is a prerequisite for successful adoption of this technology to treat other brain disorders, such as depression,[7] obsessive–compulsive disorder,[8] and epilepsy.[9]

Exploring the mechanism of action of DBS in PD patients has been exceedingly challenging. The majority of studies investigating DBS effects have been either observational or have relied upon electrophysiological techniques such as local field potentials (LFPs).[10-12] These techniques are not ideal for revealing distributed, large-scale network activity across the whole brain. Concurrent DBS–functional magnetic resonance imaging (fMRI) may provide a more comprehensive picture of stimulation-induced changes in brain networks.[13] One drawback that has hindered its use is the potential risk it poses to the brain, namely brain damage induced by electrode displacement or heating,[14] especially in the high-field MRI environment. For these reasons, previous DBS-fMRI studies were

predominantly performed in animals.[13,15] The majority of human studies have been carried out using 1.5T MRI and suffer from small sample sizes and low reliability.[16-19] However, recent advances in 3T MRI–compatible DBS technology, which can now be safely applied to humans,[20-22] has provided an unprecedented opportunity for exploring specific but subtle changes in brain circuitry induced by DBS.

Here, we aimed to explore the whole-brain effects of STN-DBS in PD patients using 3T MRI–compatible DBS. We examined the neuromodulatory effects of varying STN-DBS frequency, which accompanied changes in motor symptoms, at 4 separate postsurgical treatment visits extending over a period of 1 year (1, 3, 6, and 12 months). Importantly, we employed an fMRI block design, wherein stimulations were delivered during 36-second "ON" blocks interleaved with 24-second "OFF" blocks. This fMRI block design allowed us to directly measure brain responses to stimulation by contrasting ON versus OFF conditions. Critically, to ensure the reliability of our results, we have collected very rich neuroimaging data that are sufficient for individual-level fMRI analyses, including multiple runs ($5 \times 6$ minutes) of resting-state fMRI (rs-fMRI) during the presurgical visit and multiple runs ($8 \times 6$ minutes) of block-design fMRI data during each of the 4 postsurgical visits, totaling >220 minutes of fMRI data from each participant.

## Patients and Methods

### Participants

Fourteen patients ($54.86 \pm 7.74$ years, 9 males) with the akinetic–rigid dominant form of idiopathic PD participated in this study (mean PD duration = $9.71 \pm 3.99$ years, mean Hoehn and Yahr scale = $3.54 \pm 0.84$). See the Table for demographic and clinical characteristics. Inclusion criteria included a diagnosis of PD for >5 years, eligibility for DBS surgery, and no contraindication to MRI. More details can be found at https://clinicaltrials.gov/ct2/show/NCT02937727. This study was approved by the ethics committees of Tiantan Hospital and Peking Union Medical College Hospital in Beijing, China, and the Qilu Hospital in Jinan Shandong, China. Written informed consent was obtained from all participants. Each patient completed neurological assessments and underwent fMRI scanning approximately 1 month before DBS surgery and at 1, 3, 6, and 12 months postsurgery. Two subjects had incomplete follow-up data. No adverse events were reported.

### DBS Surgery and Neurological Assessments

All patients underwent standard frame-based stereotaxic DBS implantation surgery. For each patient, 2 quadripolar DBS electrodes (Model L301C; Beijing PINS Medical Co, Beijing, China) were implanted bilaterally into the STN, and an LFP sensing-enabled neurostimulator (G106R, Beijing PINS Medical Co) was connected to the leads (Model E202C, Beijing PINS Medical Co). Details regarding stimulation parameters for each patient at each time point are provided in Appendix S1.

The primary outcome measure of motor symptoms was obtained from scores on the motor examination portion (section III) of the Unified Parkinson Disease Rating Scale (UPDRS-III) at the presurgical and postsurgical visits. Motor symptoms were rated independently by

2 neurologists. Patients and neurologists were double-blinded to stimulation frequencies. Inter-rater reliability between evaluators' scores was evaluated using intraclass correlation coefficient (ICC).[23]

All UPDRS-III assessments were carried out when patients were in a medication OFF state for at least 12 hours. For the postsurgical visits, motor symptoms were evaluated first during a DBS OFF state. This was followed by 2 separate DBS ON states, where stimulation was delivered in either a continuous low-frequency (60Hz) or high-frequency (130Hz) mode. Importantly, to ensure a stable clinical outcome, for each stimulation mode, motor symptoms were assessed only after a 1-hour "wash-in" period, that is, symptoms were assessed after 60 minutes of continuous stimulation delivered in either the low- or high-frequency mode. The order for delivery of either low- or high-frequency stimulation experiments was pseudorandomized to control for order effects.

### MRI Safety

The challenge of investigating DBS effects on the human brain using 3T fMRI is the potential risk of brain damage caused by the possible displacement, heating, or radiofrequency-induced stimulation of the implanted DBS system. To ensure safety, our group recently investigated the displacement force, torque, and vibration of the stimulator during long-duration 3T MRI scanning.[24,25] Results demonstrated that the hazardous effect in the worst case was 0.17N for displacement force, 8mN·m for torque, and 52.4m/s$^2$ for vibration.[26] These values were only 46%, 36%, and 8% of the safety thresholds defined by the American Society for Testing and Materials[27,28] and thus met the safety requirements. The heating effect in 3T MRI was also evaluated in a phantom study[29] using fluoroptic probes. The average heating temperature recorded near an electrode was 0.4°C, well below the Health Protection Agency safety threshold (1°C).[30] In a rodent study, the integrity of brain tissue proximal to the DBS electrodes after 25 minutes of 3T MRI scanning[29] was examined histologically. No significant cellular damage was detected after hematoxylin and eosin staining, providing further evidence for the safety of the DBS stimulation system in 3T MRI.

### MRI Data Acquisition

Structural and functional MRI data were acquired with a 3T Philips (Best, the Netherlands; Achieva TX) MRI scanner equipped with a 32-channel head coil. Structural images were acquired using a sagittal magnetization-prepared rapid gradient echo T1-weighted sequence (1mm isotropic resolution, field of view [FOV] = 256, 180 slices, repetition time [TR] = 7.6 milliseconds, echo time [TE] = 3.7 milliseconds, inversion time = 1,000 milliseconds, flip angle = 8°). Functional images were acquired using an echo-planar imaging sequence (voxel size = 2.875 × 2.875 × 4mm,$^3$ FOV = 230, 37 slices, TR = 2,000 milliseconds, TE = 30 milliseconds, flip angle = 90°).

One month before surgery, a structural MRI and 5 rs-fMRI runs (6 min/run, total = 30 minutes) were acquired when patients were in a medication OFF state for at least 12 hours. Patients were instructed to relax with their eyes closed and not to fall asleep during the scan. At each of the 1-, 3-, 6-, and 12-month follow-up visits, a structural MRI and 8 functional

MRI runs (6 min/run, 4 runs for low-frequency and 4 runs for high-frequency DBS) were acquired. Each fMRI run consisted of 6 DBS ON blocks (36 s/block) interleaved with 6 DBS OFF blocks (24 s/block). Low- or high-frequency stimulation was delivered only during ON blocks. The interval between low- and high-frequency DBS-fMRI experiments was at least 1 hour to wash out effects from the previous experiment.

### DBS Lead Localization

Approximate locations of the electrodes were identified based on patients' presurgical structural MRI and postsurgical computed tomography (CT) using a protocol similar to that described by Horn and Kühn[31] with minor modifications. Specifically, postsurgical CT images were linearly coregistered to the presurgical structural MRI using SPM12 (London, UK). Presurgical magnetic resonance images were then normalized to Montreal Neurological Institute (MNI) space using Advanced Normalization Tools.[32] DBS electrode contacts were identified from the registered postsurgical CT. Approximate DBS electrode placements from all 14 patients were reconstructed in MNI space using LEAD-DBS software (Fig 1A).[31]

### Estimating DBS-Induced Frequency- and Time-Related Effects on Functional Responses

Imaging data were preprocessed using in-house software designed to remove DBS-induced noise during fMRI scanning using the following steps: (1) cortical surface was reconstructed using presurgical structural MRI (FreeSurfer); (2) postsurgical fMRI data were preprocessed using slice-timing correction and rigid-body head motion correction (FMRIB Software Library), then linearly coregistered to the presurgical structural images (FreeSurfer), and then nonlinearly registered to MNI space; (3) noise components were estimated and removed using an iterative sparse noise-modeling technique. A "nuisance mask" that included white matter, cerebrospinal fluid, and non-brain tissues was defined according to gray matter probability. Noise components were then learned from signals extracted from the nuisance mask using an iterative K-SVD algorithm.

At the first level, fMRI responses to DBS were analyzed with a block design by modeling ON versus OFF conditions as a boxcar function (see Fig 1B, C). Task activations were estimated from a general linear model (GLM) by restricted maximum likelihood approach (REML),[34] in which the noise term was modeled by first-order autoregressive process + white noise process. The resulting $\beta$-contrast maps were registered to MNI space and analyzed within subject for each stimulation frequency (low, high) and at each follow-up visit (1, 3, 6, 12 months). To quantify the test–retest reproducibility of mapping results, we partitioned each patient's fMRI data by frequency level such that each partition consisted of 2 runs (12 minutes) of fMRI data across each postsurgical time point. fMRI responses derived from 2 partitions were then compared using ICC. To examine DBS-induced functional responses at the individual level, $\beta$-contrast maps for each frequency and each time point were analyzed using a fixed-effects GLM for each patient.

A random-effects linear mixed model (LMM) analysis was performed to examine the frequency- and time-related effects of STN-DBS on whole-brain activity at the group level. $\beta$-contrast maps were fed into the second-level analysis, and served as the dependent

variable. We used a 2 (condition: low frequency, high frequency) × 4 (time: 1, 3, 6, 12 months) design, with frequency and time designated as fixed factors and subjects specified as a random effect. For the aforementioned analyses, voxels were thresholded to a $q$ value < 0.05 after false discovery rate (FDR) correction across voxels and then transformed to $z$ scores. Main effects of frequency and time, as well as their interaction, were examined separately. All subsequent post hoc comparisons were conducted using least squares means with paired $t$ tests and familywise error corrected using a Bonferroni adjustment (initial $\alpha$ = 0.05).

### rs-fMRI Analysis

Data were preprocessed using a previously published pipeline,[34] which includes (1) projecting data from the subject's native space to MNI space; (2) linear detrending and bandpass filtering (0.01–0.08Hz); (3) regressing nuisance variables, including the global signal,[35] head motion parameters, and their temporal derivatives; and (4) spatial smoothing with a Gaussian kernel of 6mm. Functional connectivity was estimated between seed regions (ie, globus pallidus internus [GPi] or motor area) and the whole brain. Group-level functional connectivity maps were computed across patients with a 1-sample $t$ test using correlation coefficients and then transformed to $z$ scores.

### Estimating DBS Frequency- and Time-Related Effects on Motor Symptom Improvement

A random-effects LMM analysis was performed on UPDRS-III scores to examine stimulation frequency- and time-dependent effects on motor symptoms. We applied a 3 (condition: DBS OFF, low frequency, high frequency) × 4 (time: 1, 3, 6, 12 months) LMM, with frequency and time entered as fixed factors and subjects designated as a random effect. All post hoc comparisons were conducted using paired $t$ tests with least squares means and corrected for multiple comparisons (Bonferroni correction, initial $\alpha$ = 0.05).

### Correlational Analyses for DBS-Induced Brain and Motor Symptom Changes

Multilevel modeling was used to ascertain whether varying DBS frequency level was predictive of changes in motor symptoms and DBS-induced (de)activations in the GPi and primary motor cortex (M1) circuits. A random-effects multilevel correlation analysis with repeated measures was performed on fMRI responses and UPDRS-III scores. For this model, stimulation frequency was specified as the predictor variable (2 levels: high, low) with repeated measures for time, and subjects designated as a random effect. The dependent variables were specified as the change (delta score) in total UPDRS-III scores for DBS ON (low [60Hz] or high [130Hz]) relative to OFF state and the change in brain responses for the GPi and M1 circuits. Change scores were graphed using scatter plots and an intrasubject correlation coefficient was calculated.

Using the same multilevel modeling approach described above, we correlated change scores from UPDRS-III subscales (tremor, rigidity, and bradykinesia) and brain responses in several regions of interest (ROIs; ie, bilateral GPi, left thalamus, M1, and anterior lobe of cerebellum). Intrasubject correlation coefficients were calculated and presented in a correlation matrix. All results were corrected for multiple comparisons using a Bonferroni adjustment (initial $\alpha$ = 0.05).

# Results

## Clinical Improvement after DBS Treatment

Motor symptom scores from the UPDRS-III showed high inter-rater reliability (ICC = 0.90); thus, the scores from 2 independent raters were averaged. Overall, patients showed significant improvement in motor symptoms as a result of continuous DBS treatment (see Fig 1D). Results from the LMM group analysis revealed a significant main effect for frequency ($F_{2,120} = 13.71$, $p < 0.001$), but not time ($F_{3,120} = 2.25$, $p = 0.09$). Post hoc comparisons (adjusted $\alpha$ level = 0.017) showed that both high- and low-frequency stimulation resulted in a significant reduction in UPDRS-III scores compared to the OFF state (130Hz vs OFF, $t_{13} = -6.45$, $p < 0.001$; 60Hz vs OFF, $t_{13} = -5.84$, $p < 0.001$) but high-frequency stimulation led to a greater improvement (130Hz vs 60Hz, $t_{13} = -3.79$, $p = 0.001$). No significant interaction between frequency and time was found ($F_{6,120} = 0.50$, $p = 0.81$).

## DBS-Induced Functional Activity Can Be Reliably Mapped at the Individual Level

Using a 3T MRI–compatible stimulator and a block-design fMRI paradigm, we were able to map the functional activity induced by STN-DBS in individual patients by contrasting the DBS ON and OFF conditions. At the single-subject level, fMRI response showed high test–retest reliability (see Fig 2 for an example). Across all 14 patients, the average reliability for low-frequency stimulation at the 1-, 3-, 6-, and 12-month visits yielded an ICC of 0.68, 0.59, 0.66, and 0.69, respectively. For high-frequency stimulation, an ICC of 0.67, 0.67, 0.69, and 0.70 at the respective time points was found. These results are more reliable than task-based fMRI results typically reported in the literature, which often fall below 0.4, as indicated in a recent meta-analysis.[36]

DBS-induced responses were estimated at the individual level using a fixed-effects model. Individual-level activation maps were variable, but there was also a high degree of consistency across patients, with activation and deactivation in regions comprising the GPi and M1 circuits, respectively (Fig 3A).

## DBS-Induced Functional Responses at the Group Level

The group-level, whole-brain LMM analysis revealed main effects for both frequency and time in 2 groups of regions (see Fig 3B). Main effects for frequency were found for the bilateral globus pallidus (GP; $F_{1,92} = 36.69$, $p < 0.001$), left thalamus ($F_{1,92} = 15.21$, $p < 0.001$), and deep cerebellar nuclei ($F_{1,92} = 9.02$, $p = 0.004$), with all structures showing strong DBS-induced activation. Significant main effects for time were found in M1 ($F_{3,92} = 54.29$, $p < 0.001$), supplementary motor area (SMA; $F_{3,92} = 26.01$, $p < 0.001$), bilateral putamen ($F_{3,92} = 23.64$, $p < 0.001$), and anterior lobe of the cerebellum ($F_{3,32} = 13.73$, $p < 0.001$), with all structures showing DBS-induced deactivation. More detailed analyses on the time and frequency effects are described in later sections. No significant interaction between frequency and time were found ($Fs_{6,92} < 0.35$, $p$'s > 0.09).

Based on the above results demonstrating a main effect of frequency for the bilateral GP, we further distinguished responses in the GP externus (GPe) and GPi by quantifying magnitude of fMRI responses at the individual level using ROIs derived from the DISTAL atlas (see Fig

3C).[37] Data were averaged across time and then contrasted for each ROI for low- versus high-frequency stimulation. Post hoc comparisons revealed that both the GPe and GPi were activated (60Hz: GPe, $t_{13}$ = 5.83; GPi, $t_{13}$ = 6.64; 130Hz: GPe, $t_{13}$ =8.45; GPi, $t_{13}$ = 9.07; $p$'s < 0.001) by low- and high-frequency DBS; however, activation was significantly greater in the GPi than GPe (60Hz: $t_{13}$ = 6.95, 130Hz: $t_{13}$ = 8.20, $p$ = 0.001; see Fig 3C).

## Activated and Deactivated Regions Represent 2 Distinct Functional Pathways

To examine whether regions (de)activated by STN-DBS were functionally dissociable, we evaluated their functional connectivity using the presurgical rs-fMRI data. Voxels showing activations thresholded with $z > 7$ in the bilateral GPi were extracted as seeds (Fig 4A). We found that the thalamus ($z$ = 4.86) and deep cerebellar nuclei ($z$ = 3.04) were functionally connected to the GPi seeds ($p < 0.01$, FDR corrected). The group activation map also overlapped with regions connected to the GPi ($Dice$ = 0.34). Similarly, we chose deactivated voxels thresholded with $z < -7$ in the M1 area as a seed (see Fig 4B) and found that the anterior lobe of cerebellum was functionally connected to the M1 ($z$ = 3.92, $p < 0.001$, FDR corrected). The deactivation map also overlapped with the M1 functional connectivity network ($Dice$ = 0.58). Importantly, the GPi and M1 networks showed little overlap with each other ($Dice$ = 0.05; see Fig 4C), indicative of 2 functionally divergent networks. Furthermore, the DBS-induced activation map shared little overlap with the M1 network ($Dice$ = 0.03), and vice versa; the DBS-induced deactivation map showed minimal overlap with the GPi network ($Dice$ = 0.07). These findings indicate that these 2 networks were not only topographically distinct, but also dissociable in terms of their response to STN-DBS.

## GPi–Thalamus–Cerebellum Circuit Is Sensitive to Stimulation Frequency

To explore the stimulation frequency effect on brain activity, group-level (de)activation maps for low- and high-frequency DBS were derived (Fig 5A). Activation of the GPi circuit varied as a function of stimulation frequency ($F_{1,92}$ = 27.75, $p < 0.001$). High-frequency stimulation induced significant activations in the bilateral GPi ($z$ = 7.37), left thalamus ($z$ = 4.61), and right deep cerebellar nuclei ($z$ = 5.30; $p < 0.01$, FDR corrected), whereas low-frequency stimulation produced activation largely restricted to the left GPi ($z$ = 3.07). The comparison between high and low frequencies revealed a significant difference in the bilateral GPi ($z$ = 5.99) and left thalamus ($z$ = 3.87; see Fig 5A, $p < 0.01$, FDR corrected). In contrast to the GPi circuit, there was no main effect of frequency for the M1 circuit ($F_{1,92}$ = 0.80, $p$ = 0.37); both low- and high-frequency stimulation induced deactivation ($p < 0.01$, FDR corrected) in M1, SMA, putamen, and anterior lobe of the cerebellum. Of particular interest was the finding that regions activated by low- and high-frequency DBS showed mild overlap ($Dice$ = 0.22), whereas deactivated regions displayed marked overlap ($Dice$ = 0.74). We then quantified average magnitude intensities in the GPi circuit and M1 circuit (see Fig 5B). Post hoc comparisons revealed greater activation in response to high- versus low-frequency for the GPi circuit ($t_{13}$=7.31, $p < 0.001$), but not the M1 circuit ($t_{13}$ =1.38, $p$ = 0.36), providing further evidence that the GPi circuit was sensitive to different stimulation frequencies.

### Deactivation in the M1–Putamen–Cerebellum Circuit Is Gradually Enhanced over Time

To examine the time-dependent effects of STN-DBS, group-level activation maps were generated at each of the 4 postsurgical visits (Fig 6A). Deactivation of the M1 circuit gradually increased over time ($F_{3,92} = 28.94$, $p < 0.001$; 1 month, $z = -1.49$; 3 months, $z = -3.95$; 6 months, $z = -5.09$; 12 months, $z = -5.94$), with no significant deactivation observed at 1 month but strong deactivation by 12 months ($Dice = 0.00$; 12 months vs 1 month, $z = 4.22$). In contrast, the GPi circuit showed sustained activation that did not differ across time $F_{3,92} = 1.74$, $p = 0.16$; 1 month, $z = 4.79$; 3 months, $z = 5.34$; 6 months, $z = 5.44$; 12 months, $z = 5.22$).

Significantly greater deactivation was observed in M1 ($z = 4.29$), putamen (left: $z = 5.90$), and anterior lobe of cerebellum ($z = 3.79$) for the 12-month relative to 1-month visit (see Fig 6A, bottom row; $p < 0.01$, FDR corrected). We then quantified average magnitude intensities in the M1 and GPi circuits. Post hoc comparisons with least squares means demonstrated that the M1 circuit showed significantly stronger deactivations at 12 months relative to 1 month ($t_{13} = -4.47$, $p < 0.001$), 3 months ($t_{13} = -3.23$, $p = 0.001$), and 6 months ($t_{13} = -1.78$, $p = 0.04$), whereas no significant differences across time were observed for the GPi circuit (see Fig 6B).

### Functional Responses in the GPi and M1 Circuits Are Associated with Different Aspects of Symptom Improvement

Our results suggest that DBS-induced activated and deactivated regions reflect 2 topographically and functionally distinct circuits that respond differently in a time- and frequency-dependent manner. The magnitude of change in response for these 2 circuits was correlated to UPDRS-III scores (Fig 7A, B). Results indicated that GPi circuit activation was significantly correlated with overall motor symptom improvement ($r = -0.42$, $p < 0.001$).

As different aspects of motor symptoms may be related to activity in divergent neural circuits, we examined the relationship between the UPDRS-III subscale measures (tremor, rigidity, and bradykinesia) and DBS-induced responses in the GPi and M1 circuits. fMRI responses were quantified in ROIs within the GPi circuit (ie, bilateral GPi and left thalamus) or M1 circuit (ie, M1 area and anterior lobe of cerebellum), and then correlated to symptom subscales (see Fig 7C). After correcting for multiple comparisons, GPi circuit activation showed a significant correlation with rigidity ($r = -0.39$, $p < 0.001$) and bradykinesia ($r = -0.37$, $p < 0.001$), whereas activation of the anterior lobe of cerebellum was correlated with reduced bradykinesia scores ($r = 0.34$, $p = 0.002$).

## Discussion

The present study examined the neuromodulatory effects of STN-DBS using 3T fMRI, afforded by recent advancements in 3T MRI–compatible DBS technology. With the advent of this new technology, we were able to explore frequency- and time-related effects of DBS at the whole-brain level in PD patients. Our results revealed 2 topographically distinct and functionally dissociable brain circuits that were differentially modulated by STN-DBS: (1) a GPi–thalamus–deep cerebellar nuclei circuit that showed marked STN-DBS–induced

activation that was frequency-dependent and (2) an M1–putamen–cerebellum circuit that showed significant STN-DBS deactivation over time. Lastly, we found that activation in the GPi circuit was associated with overall motor improvement, whereas deactivation in the M1 circuit, specifically in the cerebellum, was associated with improvement in bradykinesia, a finding that has profound implications for future biomarker development.

A key finding from the present study was that STN-DBS activated the GPi–thalamus–cerebellum circuit in a frequency-dependent manner. STN-DBS–induced GP and thalamic activation has been described in previous studies utilizing positron emission tomography (PET) and fMRI,[20,38,39] and is in accord with the classic basal ganglia–thalamus–cortex model.[40] For example, several studies employing PET have reported bilateral STN-DBS–induced increased cerebral blood flow in the GP and thalamus, which was associated with improved clinical outcomes.[41-43] A few small-scale fMRI studies have also shown STN-DBS–induced activations in the GP, thalamus, and cerebellum.[21,40] Importantly, this network was more responsive to high-frequency than low-frequency stimulation. A previous report employing computational modeling demonstrated that high-frequency DBS delivered to the STN normalized GPi firing, and reinstated thalamocortical relay responsiveness.[44] Our data also indicated that the magnitude of activation in the GPi circuit was related to motor symptom improvement. Excitatory inputs from the STN to the GPi have been identified, and together these projections comprise part of what has been termed *the indirect pathway*, with the latter nucleus providing inhibition to the thalamus, which under normal circumstances dampens activity in the motor cortex. In PD, the thalamus is thought to become overinhibited due to deficient excitatory input from the STN, which in turn leads to less motor cortex excitation and subsequent increases in aberrant motor movements.[40] As such, it seems reasonable to infer that motor symptom improvement evoked by STN-DBS in our patients may have resulted from recovery of GPi inhibitory drive on the thalamus.

Another important finding was the functional deactivation of the M1–putamen–cerebellum network that emerged over time. Results from previous neuroimaging studies characterizing M1 cortical responses to STN-DBS have been mixed. For example, Stefurak et al[45] observed significant M1 activation and SMA deactivation in a case study using an fMRI block design, a finding that is consistent with a report by Knight and colleagues.[17] In contrast, Hesselmann et al[46] showed decreased contralateral M1 activation evoked by high-frequency STN-DBS induced by a hand motor task. The inconsistent findings across studies with regard to M1 activation may be due, in part, to temporal variations in STN-DBS–induced brain responses that were not captured, and/or the timing of scanning after DBS surgery. In this study, M1 deactivation was not detectable at 1 month postsurgery, but instead appeared gradually over a period of 1 year, emerging at the 12-month visit. Our rs-fMRI results also showed that the M1–putamen–cerebellum network was functionally coupled during resting state, indicating the existence of an intrinsically connected network topographically distinct from the GPi circuit. Enhanced STN-DBS deactivation over time may reflect neuroplasticity of the M1 circuit in response to repetitive, protracted stimulation, perhaps akin to long-term depressionlike changes. Intriguingly, deactivation of the anterior lobe of the cerebellum was significantly correlated with bradykinesia improvement, suggesting an important role of the cerebellum in modulating long-term motor symptoms and progression of disease in PD.[47]

Clearly, the prognostic value of a neuroimaging biomarker for predicting motor symptom improvement, such as reflected by functional connectivity patterns,[48,49] has direct clinical implications for optimizing DBS programming strategies in individual patients. Determining the DBS parameters needed to achieve optimal therapeutic benefit is a time-consuming process, requiring many clinical visits, and resulting in significant burden for both the patient and the treating physician. This process is also extremely subjective and prone to operator error, with outcomes highly dependent upon the degree of clinical experience, which often leads to suboptimal stimulation parameters with poor symptom management. An objective predictor of treatment response such as that afforded by an fMRI biomarker would have profound implications for patient management, allowing for effective, optimal, and fast DBS programming. Although activation of the GPi and cerebellum was correlated with overall or partial improvement in motor function, whether these brain changes are able to serve as a predictive marker remains to be determined. Further validation across datasets using a prospective design is required to ascertain whether DBS-induced activation in the GPi circuit has prognostic value as an indicator of motor symptom improvement in PD patients. Additionally, more research is needed to examine the clinical implications of such biomarkers for tailoring DBS programming to patients in the clinic.

There are a few limitations in this study that deserve mention. First, our sample size was limited (n = 14). The findings are therefore subject to future replications in larger samples. Nevertheless, we acquired much longer fMRI data from each patient compared to typical fMRI studies to ensure reliability of our mapping results. High reliability is expected to increase the statistical power of group-level results. Second, we only enrolled patients with the akinetic–rigid dominant form of idiopathic PD. This is mainly based on 2 considerations: (1) in this exploratory 3T MRI study, we attempted to enroll subjects who had less head motion to ensure data quality and (2) to reduce heterogeneity of the patient sample. A follow-up study of patients with tremor-dominant symptoms is currently underway. Third, DBS-induced activity changes elicited by relatively short DBS ON (36 seconds) and OFF (24 seconds) conditions modeled during the block-design fMRI paradigm were correlated with change scores derived from the UPDRS-III, which were assessed during long, continuous low- or high-frequency stimulation relative to a baseline (OFF state). Our rationale for using an fMRI block design was to examine the rapid DBS-induced brain changes in functional activity over time and that were associated with motor symptom improvement, with the former often preceding any manifestation of observable behavioral changes. Fourth, we assessed DBS effects during the medication OFF state, which is not representative of how most patients are treated clinically, wherein DBS therapy is often used as an adjunct treatment. This was done to parse out DBS-induced functional brain changes that coincide with motor symptom improvement without the confounding effect of medication. Finally, this study examined the effect of DBS on brain networks when subjects were at rest. Future studies should explore the effect of stimulation on motor-related brain activity.[50]

In conclusion, our data revealed that STN-DBS differentially modulated 2 distinct functional circuits in PD patients. Three-tesla MRI–compatible DBS will provide unique opportunities for interrogating the highly specific structural-functional changes underlying its

neuromodulatory effects, allowing for the discovery of new therapeutic targets for a variety of neurological and psychiatric disorders.

## Supplementary Material

Refer to Web version on PubMed Central for supplementary material.

## Acknowledgment

## References

1. Benabid AL, Chabardes S, Mitrofanis J, Pollak P. Deep brain stimulation of the subthalamic nucleus for the treatment of Parkinson's disease. Lancet Neurol 2009;8:67–81. [PubMed: 19081516]

2. Bronstein JM, Tagliati M, Alterman RL, et al. Deep brain stimulation for Parkinson disease. Arch Neurol 2011;68:165. [PubMed: 20937936]

3. Volkmann J, Allert N, Voges J, et al. Safety and efficacy of pallidal or subthalamic nucleus stimulation in advanced PD. Neurology 2001;56:548–551. [PubMed: 11222806]

4. Krause M, Fogel W, Heck A, et al. Deep brain stimulation for the treatment of Parkinson's disease: subthalamic nucleus versus globus pallidus internus. J Neurol Neurosurg Psychiatry 2001;70:464–470. [PubMed: 11254768]

5. Fasano A, Romito LM, Daniele A, et al. Motor and cognitive outcome in patients with Parkinson's disease 8 years after subthalamic implants. Brain 2010;133:2664–2676. [PubMed: 20802207]

6. Moro E, Esselink RJA, Xie J, et al. The impact on Parkinson's disease of electrical parameter settings in STN stimulation. Neurology 2002;59:706–713. [PubMed: 12221161]

7. Holtzheimer PE, Husain MM, Lisanby SH, et al. Subcallosal cingulate deep brain stimulation for treatment-resistant depression: a multisite, randomised, sham-controlled trial. Lancet Psychiatry 2017;4:839–849. [PubMed: 28988904]

8. Greenberg BD, Malone DA, Friehs GM, et al. Three-year outcomes in deep brain stimulation for highly resistant obsessive-compulsive disorder. Neuropsychopharmacology 2006;31:2384–2393. [PubMed: 16855529]

9. Li MCH, Cook MJ. Deep brain stimulation for drug-resistant epilepsy. Epilepsia 2018;59:273–290. [PubMed: 29218702]

10. Bronte-Stewart H, Barberini C, Koop MM, et al. The STN beta-band profile in Parkinson's disease is stationary and shows prolonged attenuation after deep brain stimulation. Exp Neurol 2009;215:20–28. [PubMed: 18929561]

11. Kühn AA, Williams D, Kupsch A, et al. Event-related beta desynchronization in human subthalamic nucleus correlates with motor performance. Brain 2004;127:735–746. [PubMed: 14960502]

12. Brown P Oscillatory nature of human basal ganglia activity: relationship to the pathophysiology of Parkinson's disease. Mov Disord 2003;18:357–363. [PubMed: 12671940]

13. Zhao S, Li G, Tong C, et al. Full activation pattern mapping by simultaneous deep brain stimulation and fMRI with graphene fiber electrodes. Nat Commun 2020;11:1–12. [PubMed: 31911652]

14. Henderson JM, Tkach J, Phillips M, et al. Permanent neurological deficit related to magnetic resonance imaging in a patient with implanted deep brain stimulation electrodes for Parkinson's disease: case report. Neurosurgery 2005;57:E1063; discussion E1063. [PubMed: 16284543]

15. Min HK, Hwang SC, Marsh MP, et al. Deep brain stimulation induces BOLD activation in motor and non-motor networks: an fMRI comparison study of STN and EN/GPi DBS in large animals. Neuroimage 2012;63:1408–1420. [PubMed: 22967832]

16. Jech R, Urgošik D, Tint r J, et al. Functional magnetic renonance imaging during deep brain stimulation: a pilot study in four patients with Parkinson's disease. Mov Disord 2001;16:1126–1132. [PubMed: 11748747]

17. Knight EJ, Testini P, Min H, et al. Motor and nonmotor circuitry activation induced by subthalamic nucleus deep brain stimulation in patients with Parkinson disease. Mayo Clin Proc 2015;90:773–785. [PubMed: 26046412]

18. Arantes PR, Cardoso EF, Barreiros MÂ, et al. Performing functional magnetic resonance imaging in patients with Parkinson's disease treated with deep brain stimulation. Mov Disord 2006;21:1154–1162. [PubMed: 16671094]

19. Kahan J, Urner M, Moran R, et al. Resting state functional MRI in Parkinson's disease: the impact of deep brain stimulation on "effective" connectivity. Brain 2014;137:1130–1144. [PubMed: 24566670]

20. Phillips MD, Baker KB, Lowe MJ, et al. Parkinson disease: pattern of functional MR imaging activation during deep brain stimulation of subthalamic nucleus—initial experience. Radiology 2006;239:209–216. [PubMed: 16567487]

21. Sammartino F, Krishna V, Sankar T, et al. 3-Tesla MRI in patients with fully implanted deep brain stimulation devices: a preliminary study in 10 patients. J Neurosurg 2017;127:892–898. [PubMed: 28009238]

22. Boutet A, Rashid T, Hancu I, et al. Functional MRI safety and artifacts during deep brain stimulation: experience in 102 patients. Radiology 2019;293:174–183. [PubMed: 31385756]

23. Shrout PE, Fleiss JL. Intraclass correlations: uses in assessing rater reliability. Psychol Bull 1979;86:420–428. [PubMed: 18839484]

24. Jiang C, Mo X, Ding J, et al. Deep brain stimulation lead design to reduce radio-frequency heating in MRI. Electron Lett 2014;50:1898–1900.

25. Wan S Evaluation of local B1 field as dosimeter of RF heating for implant in MRI. Electron Lett 2019;55:302–304.

26. Zhang F, Jiang C, Mo X, et al. Safety assessment of displacement force, torque and vibration of a deep brain stimulation system under 3T MRI. Int J Appl Electromagn Mech 2019;59:1081–1086.

27. American Society for Testing and Materials. Standard test method for measurement of magnetically induced displacement force on medical devices in the magnetic resonance environment (F2052-06). In: Annual book of ASTM standards. West Conshohocken, PA: ASTM International, 2010:1–6.

28. American Society for Testing and Materials. Standard test method for measurement of magnetically induced torque on medical devices in the magnetic resonance environment 1. In: Annual book of ASTM standards. West Conshohocken, PA: ASTM International, 2012:1–8.

29. Wan S Research on the compatibility of deep brain stimulator in magnetic resonance imaging. PhD dissertation, 2019.

30. Health Protection Agency. Protection of patients and volunteers undergoing MRI procedures. London, UK: Health Protection Agency, 2008.

31. Horn A, Kühn AA. Lead-DBS: a toolbox for deep brain stimulation electrode localizations and visualizations. Neuroimage 2015;107:127–135. [PubMed: 25498389]

32. Avants B, Tustison N, Song G. Advanced normalization tools (ANTS). Insight J 2009;2:1–35.

33. Friston KJ, Penny W, Phillips C, et al. Classical and Bayesian inference in neuroimaging: theory. Neuroimage 2002;16:465–483. [PubMed: 12030832]

34. Li M, Wang D, Ren J, et al. Performing group-level functional image analyses based on homologous functional regions mapped in individuals. PLoS Biol 2019;17:1–27.

35. Power JD, Mitra A, Laumann TO, et al. Methods to detect, characterize, and remove motion artifact in resting state fMRI. Neuroimage 2014;84:320–341. [PubMed: 23994314]

36. Elliott ML, Knodt AR, Ireland D, et al. What is the test-retest reliability of common task-functional MRI measures? New empirical evidence and a meta-analysis. Psychol Sci 2020;31:792–806. [PubMed: 32489141]

37. Ewert S, Plettig P, Li N, et al. Toward defining deep brain stimulation targets in MNI space: a subcortical atlas based on multimodal MRI, histology and structural connectivity. Neuroimage 2018;170:271–282. [PubMed: 28536045]

38. Hilker R, Voges J, Weber T, et al. STN-DBS activates the target area in Parkinson disease: an FDG-PET study. Neurology 2008;71:708–713. [PubMed: 18650492]

39. Jech R, Kra J. Functional magnetic resonance imaging during deep brain stimulation: a pilot study in four patients with Parkinson's disease. Mov Disord 2001;16:1126–1132. [PubMed: 11748747]

40. Wichmann T, Delong MR, Guridi J, Obeso JA. Milestones in research on the pathophysiology of Parkinson's disease. Mov Disord 2011;26: 1032–1041. [PubMed: 21626548]

41. Hershey T, Revilla FJ, Wernle AR, et al. Cortical and subcortical blood flow effects of subthalamic nucleus stimulation in PD. Neurology 2003;61:816–821. [PubMed: 14504327]

42. Karimi M, Golchin N, Tabbal SD, et al. Subthalamic nucleus stimulation-induced regional blood flow responses correlate with improvement of motor signs in Parkinson disease. Brain 2008;131:2710–2719. [PubMed: 18697909]

43. Hill KK, Campbell MC, McNeely ME. Cerebral blood flow responses to dorsal and ventral STN DBS correlate with gait and balance responses in Parkinson's disease. Exp Neurol 2013;241:105–112. [PubMed: 23262122]

44. Rubin JE, Terman D. High frequency stimulation of the subthalamic nucleus eliminates pathological thalamic rhythmicity in a computational model. J Comput Neurosci 2004;16:211–235. [PubMed: 15114047]

45. Stefurak T, Mikulis D, Mayberg H, et al. Deep brain stimulation for Parkinson's disease dissociates mood and motor circuits: a functional MRI case study. Mov Disord 2003;18:1508–1516. [PubMed: 14673888]

46. Hesselmann V, Sorger B, Girnus R, et al. Intraoperative functional MRI as a new approach to monitor deep brain stimulation in Parkinson's disease. Eur Radiol 2004;14:686–690. [PubMed: 14513267]

47. Fasano A, Aquino CC, Krauss JK, et al. Axial disability and deep brain stimulation in patients with Parkinson disease. Nat Rev Neurol 2015;11:98–110. [PubMed: 25582445]

48. Horn A, Reich M, Vorwerk J, et al. Connectivity predicts deep brain stimulation outcome in Parkinson disease. Ann Neurol 2017;82:67–78. [PubMed: 28586141]

49. Horn A, Wenzel G, Irmen F, et al. Deep brain stimulation induced normalization of the human functional connectome in Parkinson's disease. Brain 2019;142:3129–3143. [PubMed: 31412106]

50. Shine JM, Matar E, Ward PB, et al. Exploring the cortical and subcortical functional magnetic resonance imaging changes associated with freezing in Parkinson's disease. Brain 2013;136:1204–1215. [PubMed: 23485851]
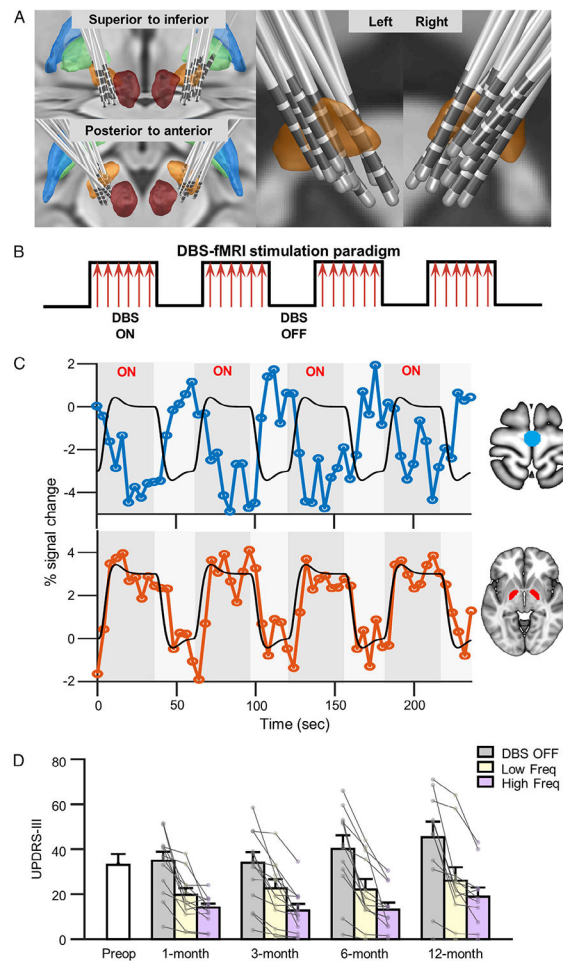
**FIGURE 1:**

Approximate electrode placement, functional magnetic resonance imaging (fMRI) stimulation paradigm, and clinical outcomes achieved by subthalamic nucleus (STN)-deep brain stimulation (DBS). (A) Approximate locations of electrodes are shown for all 14 Parkinson disease patients. Contacts for electrode lead placements were identified from postsurgical computed tomographic images and then projected onto the Montreal Neurological Institute brain template. The bilateral STN (orange), globus pallidus externus (blue), globus pallidus internus (GPi; green), and red nucleus (dark red) are shown. (B) We used a block-design fMRI stimulation paradigm. Stimulations to the bilateral STN were delivered during 36-second ON blocks followed by 24-second OFF blocks wherein no stimulation was delivered. Each fMRI run consisted of a total of 6 ON blocks and 6 OFF blocks. (C) Exemplar blood oxygen level–dependent (BOLD) signal responses from a single patient induced by high-frequency stimulation (130Hz) at the 12-month postsurgical treatment visit. Black lines depict expected percentage BOLD signal change. BOLD signal changes in the primary motor cortex (top panel; blue) and bilateral GPi (bottom panel; red) are also shown. (D) Bar graph illustrating the clinical outcome measure using total mean Unified Parkinson Disease Rating Scale, section III (UPDRS-III) scores in 14 patients, prior to (white bar) and 1, 3, 6, and 12 months following DBS surgery. Motor symptom scores using the UPDRS-III were measured during DBS OFF (baseline, gray bars) and DBS ON

states delivered at low (yellow bars) and high (pink bars) frequencies at 1, 3, 6, and 12 months postoperatively.
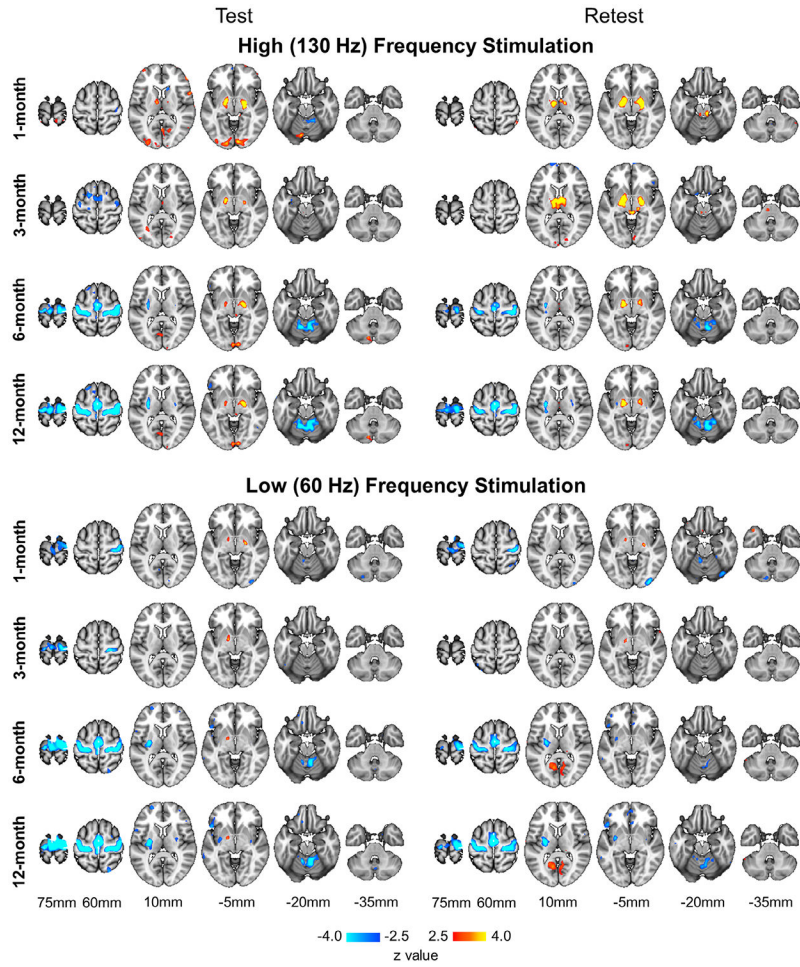
**FIGURE 2:**

Test–retest reliability of subthalamic nucleus deep brain stimulation (DBS)-induced functional magnetic resonance imaging (fMRI) responses across time. To evaluate reliability, data from each postsurgical DBS treatment visit were partitioned into 2 halves and fMRI responses were modeled using a boxcar function by contrasting the ON and OFF blocks. Test (left) and retest (right) results of an exemplar patient (Patient 13) illustrate blood oxygen level–dependent signal activations and deactivations in response to high-frequency (top panel) and low-frequency (bottom panel) DBS stimulation at the 1-, 3-, 6-, and 12-month follow-up visits.
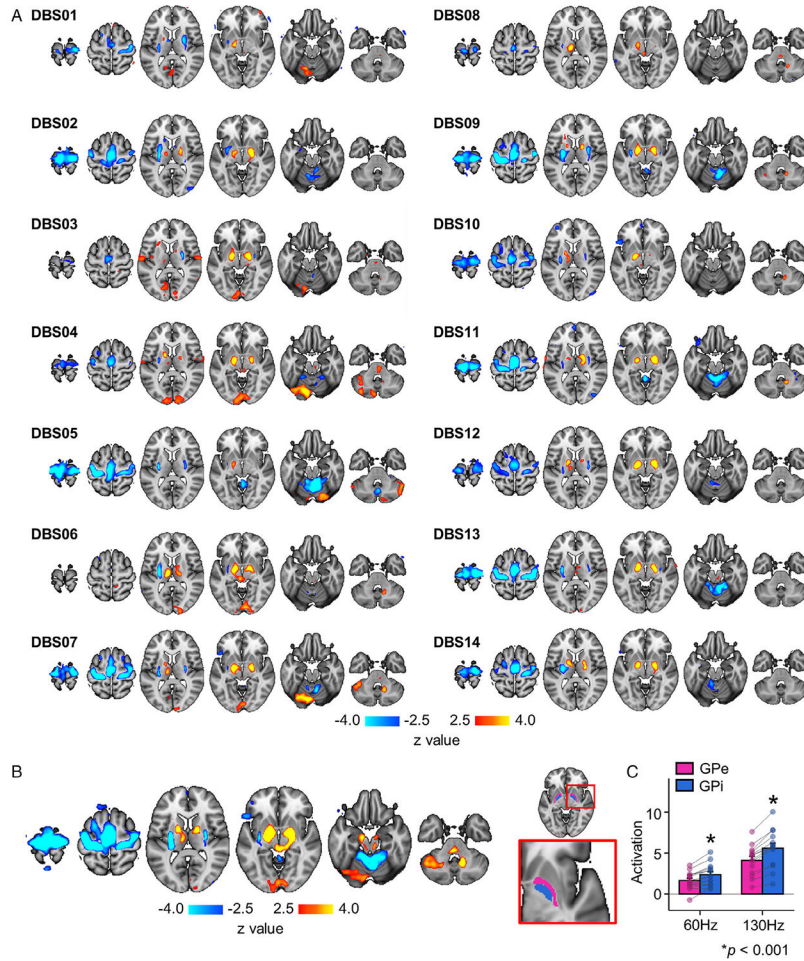
**FIGURE 3:**

Individual-level and group-level brain responses to subthalamic nucleus (STN) deep brain stimulation (DBS). (A) Responses induced by STN-DBS were estimated for each patient and overlaid onto a Montreal Neurological Institute brain template. For each patient, blood oxygen level–dependent signals corresponding to low- and high-frequency stimulation at the 1-, 3-, 6-, and 12-month follow-up treatment visits were processed by a fixed effects model. Activated regions are shown in yellow/red, and deactivated regions are shown in blue. (B) Group-level activation map was derived from a random effects linear mixed model. (C) For each patient, the magnitude of activation intensity was quantified for the globus pallidus externus (GPe; pink) and globus pallidus internus (GPi; blue; right panel). Bar graph indicates that STN-DBS–induced activation in the GPi was significantly greater at both high-frequency (130Hz) and low-frequency (60Hz) levels compared to the GPe ($p < 0.001$).
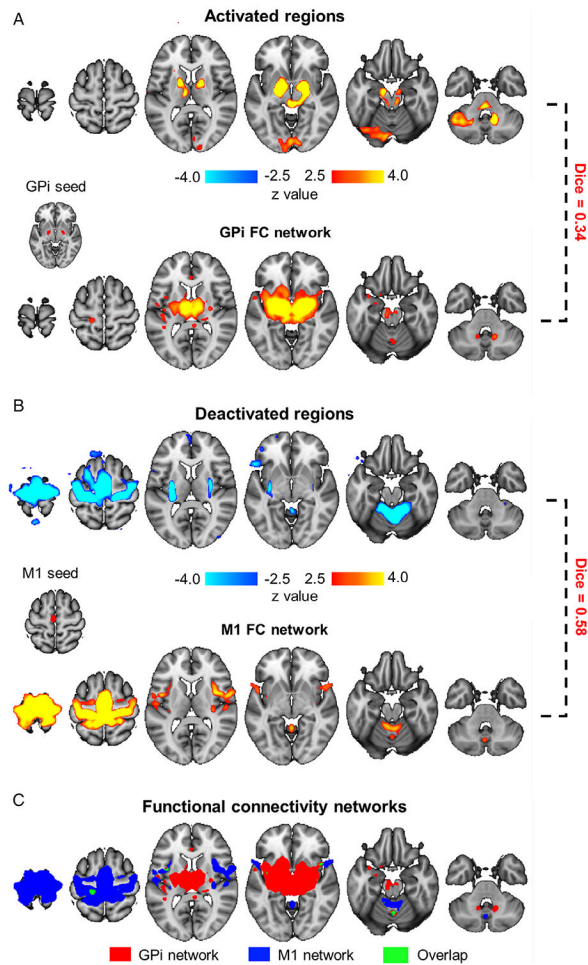
**FIGURE 4:**

Activated and deactivated regions represent 2 distinct functional pathways. (A) Group-level responses to subthalamic nucleus (STN) deep brain stimulation (DBS) showed strong activation in the globus pallidus internus (GPi), thalamus, and cerebellum (top panel). Activation peaks in the bilateral GPi ($z > 7.0$) were used as seeds (Montreal Neurological Institute [MNI] coordinates [x, y, z]: right GPi [21, −6, −1], left GPi [−17, −7, −3]), and their functional connectivity (FC) to the whole brain was estimated using presurgical resting-state functional magnetic resonance imaging data. GPi showed strong connectivity to the thalamus and deep cerebellar nuclei (bottom panel). Regions functionally connected to the GPi and regions activated by STN-DBS showed a *Dice* overlap of 0.34. (B) Group-level response to STN-DBS showed strong deactivation in primary motor cortex (M1), putamen, and cerebellum (top panel). Deactivation peaks in M1 ($z < −7.0$) were used as a seed region (MNI coordinates [x, y, z]: [−3, −17, 62]), and FC to the whole-brain was estimated (bottom panel). Regions functionally connected to M1 and regions deactivated by STN-DBS showed a *Dice* overlap of 0.58. (C) FC maps from A and B were overlaid onto a single map. Regions connected to the GPi (red) showed minimal overlap (green) with regions connected to M1 (blue), with *Dice* coefficient = 0.05.
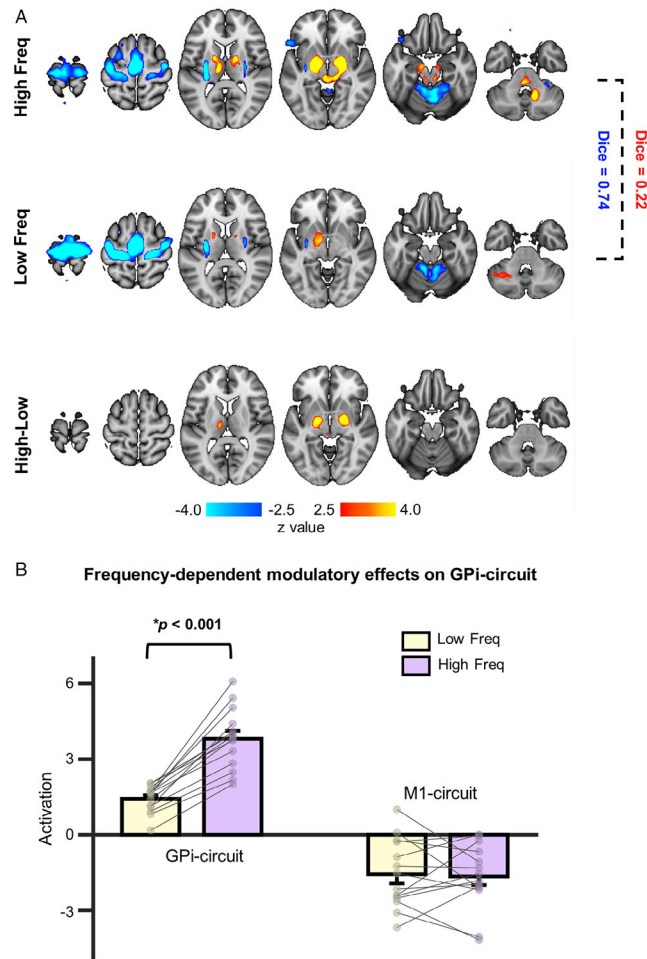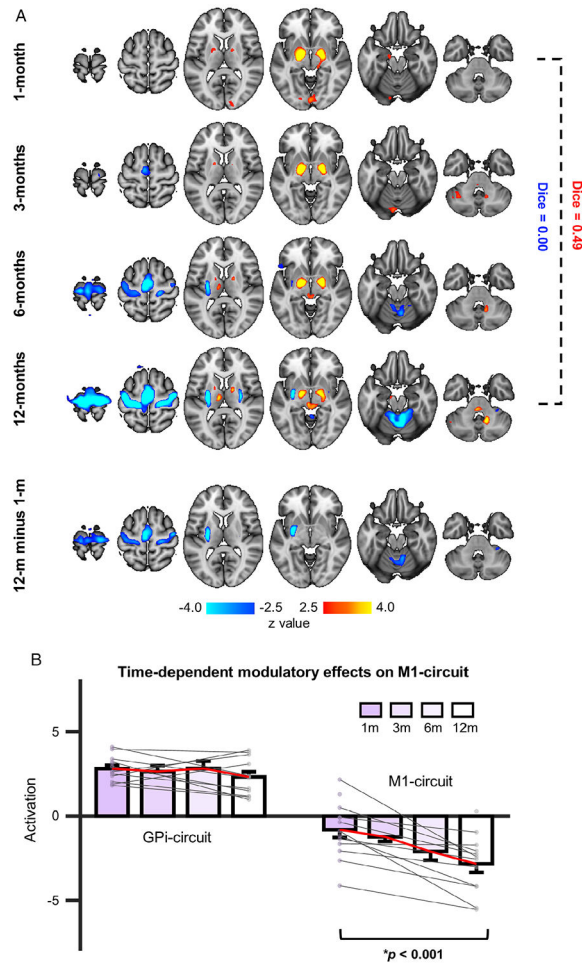
**FIGURE 5:**

The globus pallidus internus (GPi) circuit is sensitive to high-frequency stimulation. (A) Group-level brain responses to high-frequency (130Hz; top) and low-frequency stimulation (60Hz; middle) are illustrated. Regions deactivated by these 2 stimulation frequencies are highly similar (*Dice* = 0.74); however, regions activated by these 2 frequencies show minimal overlap (*Dice* = 0.22). A contrast between high- and low-stimulation frequencies indicated that activations in the GPi were significantly different (bottom). (B) Bar graphs illustrating mean magnitude of activation intensity evoked by low-frequency (60Hz; yellow bars) and high-frequency (130Hz; pink bars) deep brain stimulation, quantified in the activated GPi circuit and the deactivated primary motor cortex (M1) circuit, respectively. In the GPi circuit, blood oxygen level–dependent signal response was significantly greater for high-frequency compared to low-frequency stimulation ($p < 0.001$). No significant difference between the deactivated M1 circuit for these 2 stimulation frequencies was found ($p = 0.36$).

**FIGURE 6:**

Subthalamic nucleus (STN) deep brain stimulation (DBS) treatment resulted in gradual and sustained increases in the primary motor cortex (M1) circuit deactivation over time. (A) Group-level responses induced by STN-DBS were estimated for each postsurgical treatment visit (top 4 rows). Regions activated by STN-DBS (red/yellow) were relatively stable across the 4 follow-up visits. Activated regions at 1 month and 12 months were highly similar (*Dice* = 0.49). However, deactivation (blue) in the M1 circuit was gradually enhanced over time. There was no significant deactivation at 1 month postsurgery, but prominent deactivations at 12 months were observed (*Dice* = 0.00). Group-level comparison between blood oxygen level–dependent signal responses at 1-versus 12-month visits revealed a significant difference in deactivation but not activation levels (bottom panel). (B) Mean magnitude of activation intensity was quantified in the activated globus pallidus internus (GPi) circuit and the deactivated M1 circuit at each visit. A linear mixed model analysis revealed that the intensity of the activations was stable over time, as there was no significant main effect of time ($p = 0.16$). However, deactivations showed a significant time effect ($F_{3,92} = 25.59$, $p < 0.001$).
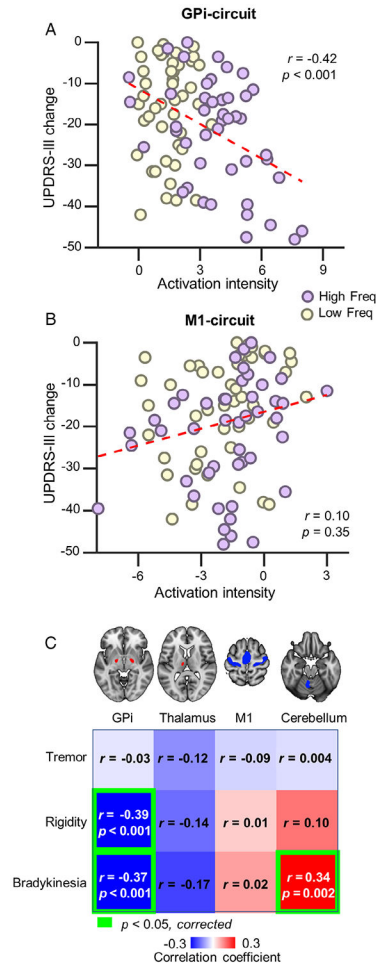
**FIGURE 7:**

Functional responses in 2 dissociable circuits are associated with different aspects of symptom improvements. (A) The scatterplot illustrates a significant correlation ($r = -0.42$, $p < 0.001$) between clinical outcome as measured by Unified Parkinson Disease Rating Scale, section III (UPDRS-III) change scores (UPDRS-III scores during deep brain stimulation [DBS] ON vs DBS OFF; ON minus OFF) and the magnitude of functional response in the activated globus pallidus internus (GPi) circuit. (B) The correlation between magnitude of deactivation in the primary motor cortex (M1) circuit and motor symptom scores on the UPDRS-III was not significant ($r = 0.10$, $p = 0.35$). (C) Correlation coefficients between (de)activation magnitude extracted from regions of interest (from left to right: the bilateral GPi, left thalamus, M1, and anterior lobe of cerebellum) and clinical outcome as measured by UPDRS-III subscales (from top to bottom: tremor, rigidity, and bradykinesia) presented as a correlation matrix (red = positive correlation; blue = negative correlation). Significant correlations (Bonferroni adjusted) are highlighted using green frames. Activation in GPi was correlated with rigidity and bradykinesia, whereas deactivation in the cerebellum was correlated with bradykinesia.

**TABLE.**

Clinical Characteristics

| Patient ID | Age, yr | Gender | Education, yr | MMSE | H-Y | PD Duration, yr | UPDRS-III, Presurgical | PDQ-39 |
|---|---|---|---|---|---|---|---|---|
| DBS01 | 40 | M | 9 | 26 | 3 | 8 | 22 | 75 |
| DBS02 | 53 | M | 12 | 25 | 3 | 13 | 34 | 34 |
| DBS03 | 67 | M | 12 | 27 | 3 | 8 | 21 | 78 |
| DBS04 | 51 | M | 12 | 27 | 4 | 20 | 20 | 40 |
| DBS05 | 65 | M | 12 | 28 | 3 | 6 | 21 | 14 |
| DBS06 | 60 | F | 9 | 28 | 3 | 7 | 29 | 71 |
| DBS07 | 46 | M | 15 | 29 | 4 | 7 | 47 | 60 |
| DBS08 | 59 | M | 6 | 28 | 4 | 10 | 40 | 51 |
| DBS09 | 61 | F | 6 | 28 | 4 | 8 | 29 | 51 |
| DBS10 | 51 | M | 15 | 28 | 1.5 | 6 | 8 | 75 |
| DBS11 | 47 | F | 9 | 28 | 5 | 12 | 38 | 68 |
| DBS12 | 56 | F | 15 | 26 | 4 | 15 | 51 | 61 |
| DBS13 | 61 | F | 9 | 30 | 4 | 8 | 41 | 127 |
| DBS14 | 51 | M | 12 | 30 | 4 | 8 | 54 | 39 |
| Mean | 54.9 | 5 F/9 M | 10.9 | 27.7 | 3.5 | 9.7 | 32.3 | 60.3 |
| SD | 7.7 | | 3.0 | 1.4 | 0.8 | 4.0 | 13.3 | 26.7 |

F = female; H-Y = Hoehn and Yahr scale; M = male; MMSE = Mini-Mental State Examination; PD = Parkinson disease; PDQ = Parkinson's Disease Questionnaire; SD = standard deviation; UPDRS-III = Unified Parkinson Disease Rating Scale, section III.